chemosensors

MDPI

Article

A Long-Wavelength Fluorescent Probe for Efficient Dual-Color Imaging of Boronic-Acid-Containing Agents in Living Cells

Shinya Takada [1,2], Honghuo Du [2], Naoya Kondo [2,3], Anna Miyazaki [2], Fumiko Hara [1], Shizuyo Horiyama [1], Takashi Temma [2,4,*] and Masayori Hagimori [1,*]

[1] Laboratory of Analytical Chemistry, Faculty of Pharmaceutical Sciences, Mukogawa Women's University, Nishinomiya 663-8179, Japan; takada_shinya_x@mukogawa-u.ac.jp (S.T.); fhara@mukogawa-u.ac.jp (F.H.); horiyama@mukogawa-u.ac.jp (S.H.)

[2] Department of Biofunctional Analysis, Graduate School of Pharmaceutical Sciences, Osaka Medical and Pharmaceutical University, Takatsuki 569-1094, Japan; kondon@hirakata.kmu.ac.jp (N.K.); anna.miyazaki@ompu.ac.jp (A.M.)

[3] Division of Fundamental Technology Development, Near InfraRed Photo-ImmunoTherapy Research Institute, Kansai Medical University, Hirakata 573-1010, Japan

[4] Particle Radiation Biology, Institute for Integrated Radiation and Nuclear Science, Kyoto University, Sennan-gun 590-0494, Japan

* Correspondence: temma.takashi.3s@kyoto-u.ac.jp (T.T.); hagimori@mukogawa-u.ac.jp (M.H.)

Abstract

In boron neutron capture therapy (BNCT), the intracellular localization and concentration of boron-10 atoms significantly influence therapeutic efficacy. Although various boronic-acid-targeted fluorescent probes have been developed to evaluate BNCT agents, most of these probes emit at short wavelengths and are, therefore, incompatible with common nuclear-staining reagents such as Hoechst 33342 and 4′,6-diamidino-2-phenylindole (DAPI). While our previously reported probe, BS-631, emitted fluorescence above 500 nm, it exhibited limitations in terms of reaction rate and fluorescence intensity. To address these issues, we developed a boronic-acid-targeted fluorescent probe with a longer emission wavelength, rapid reactivity, and strong fluorescence intensity. Herein, we designed and synthesized BTTQ, a probe based on a 2-(2-hydroxyphenyl)benzothiazole core structure. BTTQ exhibited immediate fluorescence upon reaction with 4-borono-L-phenylalanine (BPA), with an emission wavelength of 567 nm and a sufficiently high fluorescence quantum yield for detection. BTTQ quantitatively detected BPA with high sensitivity (quantification limit of 10.27 μM), suitable for evaluating BNCT agents. In addition, BTTQ exhibited selective fluorescence for BPA over metal cations. Importantly, BTTQ enabled fluorescence microscopic imaging of intracellular BPA distribution in living cells co-stained with Hoechst 33342. These results suggest that BTTQ is a promising fluorescent probe for the evaluation of future BNCT agents.

Keywords: BNCT; boronic acid; fluorescent probe; cancer; BPA

check for updates

Received: 27 June 2025
Revised: 25 July 2025
Accepted: 31 July 2025
Published: 4 August 2025

Citation: Takada, S.; Du, H.; Kondo, N.; Miyazaki, A.; Hara, F.; Horiyama, S.; Temma, T.; Hagimori, M. A Long-Wavelength Fluorescent Probe for Efficient Dual-Color Imaging of Boronic-Acid-Containing Agents in Living Cells. *Chemosensors* **2025**, *13*, 283. https://doi.org/10.3390/chemosensors13080283

Copyright: © 2025 by the authors. Licensee MDPI, Basel, Switzerland. This article is an open access article distributed under the terms and conditions of the Creative Commons Attribution (CC BY) license (https://creativecommons.org/licenses/by/4.0/).

1. Introduction

Boron neutron capture therapy (BNCT) is a cancer treatment method that utilizes the nuclear reaction between boron-10 (^{10}B) atoms and thermal neutrons to generate high-linear-energy-transfer (LET) radiation, such as alpha particles (^{4}He) and recoiling ^{7}Li nuclei [1,2]. Consequently, various ^{10}B-containing compounds have been successfully developed for BNCT [3,4]. In Japan, 4-borono-L-phenylalanine (BPA, Steboronine®) was approved for clinical use in BNCT in 2020 and remains the only BNCT agent currently

employed [5,6]. BPA is taken up by cancer cells via L-type amino acid transporter 1 (LAT1), which is highly expressed in many tumors [7,8]. Real-world clinical data from 2020 have demonstrated promising outcomes of BPA-based BNCT [6,9]. However, BPA has limitations in terms of tumor specificity and water solubility [10,11]. Consequently, intensive research is ongoing to develop next-generation ^{10}B-containing compounds with improved characteristics [10,12–15]. In this context, boronic acid derivatives, such as BPA, are anticipated to play a pivotal role as fundamental ^{10}B-containing moieties in the design of novel boron agents.

BNCT exerts its therapeutic effect by inducing double-strand DNA damage through high-LET radiation with an extremely short range (4–10 μm) [16,17]. Thus, the intracellular localization and concentration of ^{10}B in cancer cells significantly influence the therapeutic efficacy of BNCT [18,19]. Consequently, accurate analysis of the intracellular distribution and quantity of ^{10}B is a critical step in the development of effective BNCT agents. To date, the localization of ^{10}B in tissue sections has been analyzed by laser ablation inductively coupled plasma mass spectrometry (LA-ICP-MS); however, cellular analyses have not yet been performed [20]. Secondary ion mass spectrometry (SIMS) can provide cellular-level localization of ^{10}B but requires sample pretreatment and cannot be applied to live cells [21,22].

Fluorescent probes are widely used as versatile analytical tools for detecting targets in living cells [23–25]. Recently, we reported BITQ, a boronic-acid-targeted fluorescent probe (Figure 1) [26]. BITQ exhibits rapid reactivity with boronic acids and demonstrates a sufficiently high quantum yield (>10%), enabling intracellular imaging of BPA. However, upon reaction with BPA, BITQ emits fluorescence at 480 nm, which overlaps with the emission wavelengths of commonly used nuclear-staining reagents such as Hoechst 33342 (λ_{em} = 461 nm) and 4′,6-diamidino-2-phenylindole (DAPI) (λ_{em} = 460 nm). This spectral overlap limits their application in multicolor imaging. Therefore, specialized probes that emit green or red fluorescence are required for simultaneous nuclear staining. Previously, we reported on BS-631, a red-emitting boronic-acid-targeted fluorescent probe compatible with Hoechst 33342 (Figure 1) [27]. Although BS-631 allows dual-color imaging, it exhibits a slow reaction rate with BPA and relatively low fluorescence intensity. To address these limitations, we aimed to develop a novel small-molecule boronic-acid-targeted fluorescent probe that exhibits long-wavelength fluorescence (>500 nm), rapid reactivity, and high fluorescence intensity.

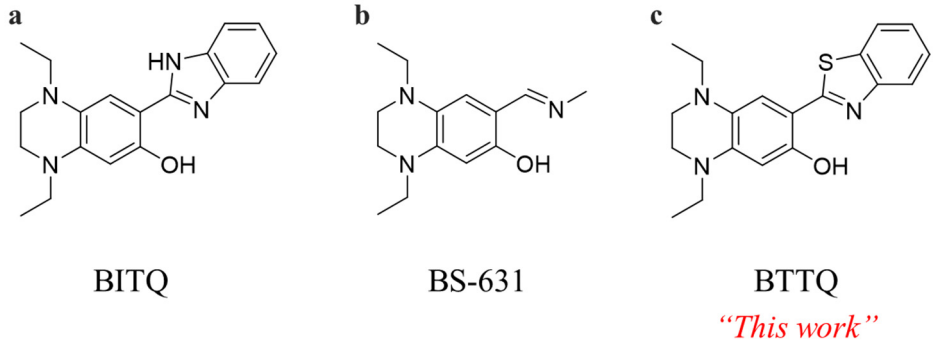


Figure 1. Chemical structures of (**a**) BITQ [26], (**b**) BS-631 [27], and (**c**) BTTQ.

Herein, 2-(2-hydroxyphenyl)benzothiazole (HBT) was selected as the core skeleton because it is expected to react rapidly and exhibit favorable fluorescence properties. HBT has a longer fluorescence emission wavelength (λem = 480 nm) than 2-(2-hydroxyphenyl)-*1H*-benzimidazole (λem = 460 nm) [28,29], which is the core structure of BITQ. The boronic acid chelation site in HBT consists of a heterocyclic nitrogen-containing ring and a phenolic hydroxyl group. Although HBT exhibits a low quantum yield (<1%), previous

reports have shown that chelation with boron trifluoride significantly improves its quantum yield (>20%) [30], suggesting that structural conversion induced by a reaction with boron agents can lead to a high post-to-pre-fluorescence intensity ratio. Therefore, we designed the probe by introducing a tetrahydroquinoxaline (TQ) moiety, which is a strong electron-donating group known to extend the emission wavelength of fluorescent molecules (Figures 1 and 2) [26,31,32]. In this study, we synthesized BTTQ, evaluated the changes in its fluorescence properties in response to BPA, and investigated its ability to visualize the intracellular localization of BPA.

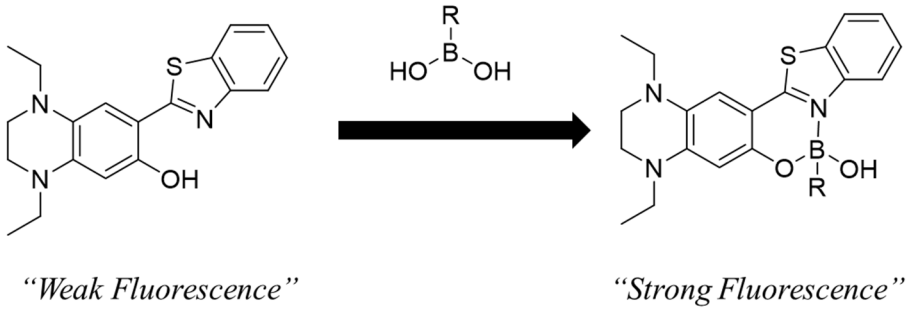


Figure 2. Schematic diagram of boronic acid detection by fluorescent complexes of BTTQ and boronic acid compounds.

2. Materials and Methods

2.1. Reagents and Instruments

All solvents and reagents were purchased from Tokyo Chemical Industry (Tokyo, Japan), Nacalai Tesque (Kyoto, Japan), FUJIFILM Wako Pure Chemical Industry (Osaka, Japan), and Alfa Aesar (Ward Hill, MA, USA), and used without purification. BPA was supplied by Stella Pharma K.K. (Osaka, Japan) or purchased from BLDpharm (Shanghai, China). Fluorescence analysis was performed using spectroscopic analysis-grade solvents and ultrapure water. Separation and purification were performed using a Selekt Enkel flash column chromatography system (Biotage, Tokyo, Japan). Mass spectra (MS) and high-resolution mass spectra (HRMS) were measured with a JMS-700 mass spectrometer (JEOL Ltd., Tokyo, Japan). ^{1}H- and ^{13}C-NMR spectra were measured with a JEOL ECA-500 NMR system (JEOL Ltd., Tokyo, Japan, 500 MHz). Tetramethylsilane was used as the 0 ppm standard for the NMR measurements. Emission spectra and fluorescence intensity were measured on an FP-8600 or FP-8300 spectrometer (JASCO Corporation, Tokyo, Japan). The absolute quantum yield was measured with an FP-8300 spectrometer and an ILF-835 integrating sphere (JASCO Corporation, Tokyo, Japan).

2.2. Synthesis of BTTQ

Intermediates of BTTQ and BTTQ were synthesized following previous reports, with minor modifications [26,27]. To a solution of 0.20 g of 1,4-Diethyl-7-hydroxy-1,2,3,4-tetrahydroquinoxaline-6-carbaldehyde (0.85 mmol) in N,N-dimethylformamide (DMF) (2.0 mL), 2-aminobenzenethiol (0.11 g, 0.88 mmol) was added. The mixture was stirred at room temperature for 1 min; then, 0.5 mL of ultrapure water containing 0.24 g of sodium metabisulfite (1.26 mmol) was added to the mixture. After the reaction mixture was stirred at 90 °C for 4 h, ice-cold water (50 mL) was added and extracted with ethyl acetate (150 mL). The ethyl acetate layer was separated and anhydrous $MgSO_4$ was added for drying, then concentrated under reduced pressure. The BTTQ (0.14 g, 48%) was obtained by silica gel chromatography (ethyl acetate/hexane) as an orange solid.

^{1}H-NMR (500 MHz, DMSO-d_6) δ: 1.08–1.16 (m, 6H), 3.14–3.16 (t, 2H, J = 5.0 Hz), 3.26–3.30 (q, 2H, J = 7.0 Hz), 3.30–3.37 (m, 2H), 3.43–3.45 (t, 2H, J = 4.5 Hz), 6.14 (s, 1H), 6.85

(s, 1H), 7.30–7.33 (t, 1H, *J* = 7.5 Hz), 7.43–7.46 (t, 1H, *J* = 7.5 Hz), 7.87–7.88 (d, 1H, *J* = 8.0 Hz), 7.99–8.01 (d, 1H, *J* = 8.0 Hz), 11.27 (s, 1H).

^{13}C-NMR (125 MHz, DMSO-d_6) δ: 9.5, 10.1, 44.6, 44.6, 44.7, 46.7, 96.6, 104.6, 108.3, 120.5, 121.5, 123.7, 126.2, 128.3, 132.3, 140.5, 151.8, 151.8, 167.4.

EI-MS *m*/*z*: 339. Found: 339. HRMS (EI) *m*/*z*: Calcd. for $C_{19}H_{21}N_3OS$ M^+: 339.1405. Found: 339.1407.

2.3. Fluorescence Properties

BTTQ was prepared as a 10 mM stock solution in DMSO. BTTQ and BPA were mixed in 0.5% DMSO/H_2O to final concentrations of 10 μM and 1000 μM, respectively. After 5 min, the spectral profiles of the excitation and emission data were recorded with an FP-8600 spectrometer (photomultiplier tube [PMT] voltage: 1000 V) to determine the maximum excitation (λex-max) and emission (λem-max) wavelengths.

BTTQ and BPA were also mixed in 0.5% DMSO/phosphate buffer (50 mM, pH 6.0–8.0) to final concentrations of 10 μM and 100 μM, respectively. Five minutes after mixing, fluorescence intensities were recorded using a spectrometer (λex/λem: 430/567 nm; FP-8300 spectrometer; PMT voltage: 300 V; *n* = 3).

BTTQ and BPA were also mixed in 25% or 50% DMSO/H_2O to achieve final concentrations of 10 μM for BTTQ and 1000 μM for BPA. After 5 min, the emission spectra were measured with an FP-8300 spectrometer (PMT voltage: 300 V).

Further, BTTQ and phenylboronic acid (PBA) were mixed in ethanol to achieve final concentrations of 20 μM for BTTQ and 10,000 μM for PBA. Five minutes later, the emission spectrum was measured at an excitation wavelength (430 nm) to calculate the absolute quantum yield using an FP-8300 spectrometer equipped with an ILF-835 integrating sphere (PMT voltage: 250 V, *n* = 3).

2.4. Reactivity Assay with Other Boronic-Acid-Containing Compounds

BTTQ was mixed with various boronic-acid-containing compounds (boric acid, ethylboronic acid, 4-carboxyphenyl boronic acid, or 2-(hydroxymethyl)phenylboronic acid cyclic monoester) in 0.5% DMSO/H_2O to final concentrations of 10 μM and 100 μM, respectively. After 5 min, the emission spectra were measured using a spectrometer (λex: 430 nm; FP-8300 spectrometer; PMT voltage: 300 V).

2.5. Temporal Changes in Fluorescence Intensity

BTTQ and BPA were mixed in 0.5% DMSO/H_2O to final concentrations of 10 μM and 1000 μM, respectively, and fluorescence intensity (λex/λem: 430/567 nm; FP-8600 spectrometer; PMT voltage: 1000 V) was measured at intervals for 30 min post-addition (*n* = 3).

2.6. Detection and Quantification Limits

BTTQ and BPA were mixed in 0.5% DMSO/H_2O to final concentrations of 10 μM and 0–1000 μM, respectively. Five min after mixing, fluorescence intensities were recorded with a spectrometer (λex/λem: 430/567 nm; FP-8600 spectrometer; PMT voltage: 1000 V; *n* = 5). We performed linear regression analysis on the obtained data at each BPA concentration, and the detection and quantification limits were calculated using the following equations:

$$\text{Detection limit} = 3\ \sigma/\text{slope}$$

$$\text{Quantification limit} = 10\ \sigma/\text{slope}$$

In this equation, the slope was obtained from the regression line, and σ is the standard deviation of the fluorescence intensity of the sample at 10 μM of BTTQ and 0 μM of BPA.

2.7. Selectivity Assay

BTTQ and BPA or a metal chloride (NaCl, $MgCl_2 \cdot 6H_2O$, $AlCl_3 \cdot 6H_2O$, KCl, $CaCl_2$, $MnCl_2 \cdot 4H_2O$, $FeCl_2 \cdot 4H_2O$, $FeCl_3 \cdot 6H_2O$, $CoCl_2 \cdot 6H_2O$, $NiCl_2 \cdot 6H_2O$, $CuCl_2 \cdot 2H_2O$, $ZnCl_2$, or $CdCl_2 \cdot 2.5H_2O$) were mixed in 0.5% DMSO/H_2O to give final concentrations of 10 μM for BTTQ and 100 μM each for BPA and the metal chloride. Five min after mixing, fluorescence intensities were recorded with a spectrometer (λex/λem: 430/567 nm; FP-8300 spectrometer; PMT voltage: 300 V; n = 3). The fluorescence intensities were expressed as a relative value to that of the BTTQ solution without the addition of metal chlorides and BPA, at 100%.

BTTQ, BPA, and each of the abovementioned metal chlorides were mixed in 0.5% DMSO/H_2O to final concentrations of 10 μM, 100 μM, and 100 μM, respectively. The measurements were taken under the same conditions as above, and the results were expressed as relative values to that of the BTTQ solution without the addition of metal chlorides and BPA, at 100% (n = 3).

BTTQ (final concentration: 10 μM) and BPA (final concentration: 100 μM), and $FeCl_3 \cdot 6H_2O$ (final concentration of 0, 1, 10, or 100 μM), were mixed in 0.5% DMSO/H_2O.

The fluorescence intensity was measured 5 min after mixing under the same conditions as above and compared with that of a BTTQ-BPA solution (10 μM and 100 μM, respectively) without $FeCl_3 \cdot 6H_2O$ (n = 3).

2.8. Fluorescence Microscopy Study

Human pancreatic adenocarcinoma cells (T3M-4) were provided by the RIKEN BioResource Research Center (Ibaraki, Japan). T3M-4 cells were cultured in DMEM/Ham's F-12 medium containing 5% penicillin-streptomycin and 10% fetal bovine serum at 37 °C in a humidified atmosphere of 5% CO_2. The procedure for BPA uptake was based on a previously published protocol [26], with minor modifications.

T3M-4 cells were seeded onto 35 mm glass-bottom dishes (D11130H, Matsunami Glass Ind., Osaka, Japan) and cultured for 2 days prior to the study. The cells were washed three times with 1 mL of Na^+-free Hank's balanced salt solution (HBSS: 1.2 mM KH_2PO_4, 1.2 mM $MgSO_4$, 1.3 mM $CaCl_2$, 5.6 mM D-glucose, 4.8 mM KCl, 25 mM HEPES, and 125 mM choline chloride), after which 1.5 mL of BPA-Fructose (1.0 mM in HBSS) was added. Cells were then incubated at 37 °C for 30 min. For the group without the addition of BPA, only HBSS was added, and the solution was incubated under conditions identical to those used for the BPA additive group. Following three additional washes with HBSS (1 mL), 10 μM of BTTQ solution (1.5 mL) in 0.5% DMSO/HBSS was added, and cells were incubated at room temperature for 5 min. Finally, after washing three times with 1 mL of HBSS, for nucleus staining, cells were incubated with Hoechst 33342 (100 μg/mL) at 37 °C for 30 min. Fluorescence images were captured using a BZ-X810 microscope (Keyence, Osaka, Japan) equipped with a DAPI filter cube (Keyence OP-87762; Ex: 360 ± 20 nm; Em: 460 ± 25 nm) for Hoechst 33342 and a GFP filter cube (Keyence OP-87763; Ex: 470 ± 20 nm; Em: 525 ± 25 nm) for BTTQ.

3. Results and Discussion

3.1. Fluorescence Properties of BTTQ

BTTQ was synthesized in six steps, with an overall yield of 15%. As expected, BTTQ exhibited a 20-fold increase in fluorescence intensity upon reaction with BPA (Figure 3). As summarized in Table 1, the maximum excitation (λex-max) and emission wavelengths (λem-max) of BTTQ after BPA addition were 430 nm and 567 nm, respectively (Figures 3 and S5). These values are red-shifted compared to those of BITQ (λex-max: 390 nm; λem-max: 480 nm) and are more compatible with the GFP filter cube than those of BS-631 [26,27].

Furthermore, the maximum excitation wavelength of BTTQ exceeds 400 nm, placing it outside the ultraviolet range, which may help reduce phototoxicity during live-cell imaging. BTTQ also exhibits a large Stokes shift of 137 nm, which is greater than that of conventional fluorescent dyes [33,34], thereby minimizing interference from the excitation light in fluorescence microscopy.

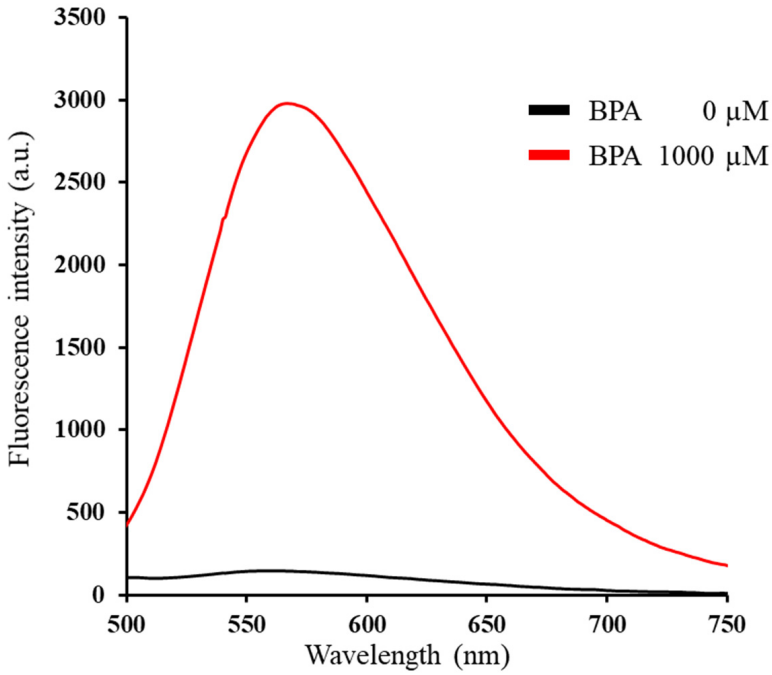


Figure 3. Emission spectra of BTTQ (10 μM) in 0.5% DMSO/H_2O 5 min after addition of BPA (0 or 1000 μM) (FP-8600 spectrometer; λex: 430 nm).

Table 1. Fluorescence properties of BTTQ.

Compound	$\lambda_{ex\text{-}max}$	$\lambda_{em\text{-}max}$	Stokes Shift	φ_{boron}	$\varphi_{boron}/\varphi_{Free}$
BTTQ	430 nm	567 nm	137 nm	19%	19

To evaluate the effect of pH on the BPA detection ability of BTTQ, the fluorescence intensity at 567 nm was measured at an excitation wavelength of 430 nm in 0.5% DMSO/phosphate buffer solutions (50 mM) with different pH ranges (pH 6.0–8.0) (Figure S6). In the group without the addition of BPA, the fluorescence intensity increased gradually with pH; however, upon the addition of BPA, the fluorescence intensity increased more than two-fold across all tested pH values and remained stable throughout. These results indicate that BTTQ is capable of detecting BPA under physiological conditions.

The absolute quantum yield of BTTQ alone was 1.01% ± 0.04%, which increased to 19.1% ± 0.44% upon addition of PBA, indicating a sufficient fluorescence response for the detection of boronic acid compounds. In contrast, the previously reported BITQ exhibited a higher quantum yield of 53% after PBA addition; however, it also exhibited strong background fluorescence in the absence of PBA. As a result, the post-to-pre-quantum yield ratio of BITQ was relatively low at only 5.6-fold. Conversely, BTTQ displayed very weak background fluorescence, leading to a significantly higher 19-fold post-to-pre-quantum yield ratio. This suggests that BTTQ functions as an effective OFF/ON switching-type fluorescent probe with superior signal contrast. Also, EI-MS analysis of the mixture of BTTQ and phenylboronic acid revealed mass values suggestive of a complex between BTTQ and phenylboronic acid (Figure S4). $C_{25}H_{25}BN_3OS$ $[M\text{-}OH]^+$: 426.1811. Found: 426.1812. This

result suggests that BTTQ undergoes a fluorescence change via the mechanism outlined in Figure 2.

Recently, Sun et al. reported that the addition of BPA to HBT in 50% DMSO/PBS did not induce any changes in the emission spectra [35]. Consistent with this, the HBT-based probe, BTTQ, also showed no fluorescence change upon the addition of BPA in 50% DMSO/H_2O (Figure S7). However, when the DMSO content was reduced to 25%, a marked increase in BTTQ fluorescence was observed upon the addition of BPA (Figure S7). Although the precise mechanism by which DMSO affects BTTQ's fluorescence response remains unclear, these results demonstrate that BTTQ is capable of detecting BPA under more aqueous conditions. This suggests its potential applicability in live-cell fluorescence imaging.

When other boronic-acid-containing compounds were mixed with BTTQ, minimal fluorescence enhancement was observed for boric acid and ethylboronic acid. In contrast, the fluorescence intensity increased significantly with 4-carboxyphenylboronic acid and 2-(hydroxymethyl)phenylboronic acid cyclic monoester. These results suggest that BTTQ preferentially detects boronic-acid-containing compounds bearing benzene rings (Figure S8).

Temporal changes in the fluorescence intensity of BTTQ are shown in Figure 4. Upon the addition of BPA, the fluorescence intensity of BTTQ rapidly increased, reaching a maximum within 1 min, and remained stable for at least 30 min thereafter. In contrast, BS-631 has been reported to require more than 60 min to react with boronic acids [27]. These results indicate that BTTQ offers a faster response and greater stability, making it more suitable than BS-631 for time-sensitive quantitative analyses in in vitro studies, such as time-dependent uptake experiments used to evaluate the effectiveness of BNCT agents.

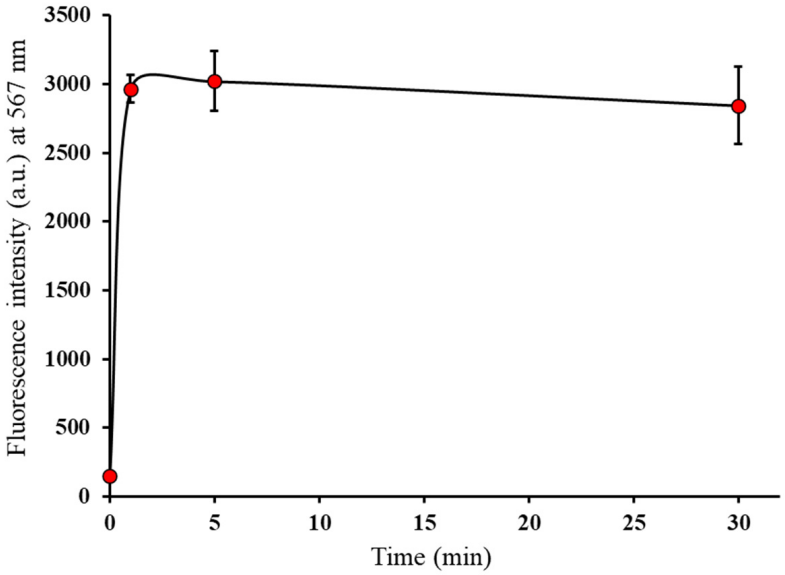


Figure 4. Temporal change in fluorescence intensities of BTTQ (10 μM) after BPA (1000 μM) addition in 0.5% DMSO/H_2O (FP-8600 spectrometer; λex/λem: 430/567 nm).

Linear regression analysis revealed a strong correlation between BTTQ fluorescence intensity and BPA concentration over the range of 0–1000 μM (r = 0.999, Figure 5). Based on this, the detection limit and quantification limit of BTTQ for BPA were calculated to be 3.08 μM and 10.27 μM, respectively. While these values are higher than those reported for BITQ (detection limit, 0.24 μM; quantification limit, 0.82 μM), they are significantly lower than those of BS-631 (detection limit, 19.6 μM; quantification limit, 65.3 μM). Considering that the minimum effective intratumoral ^{10}B concentration required for successful BNCT

exceeds 2 mM, the detection and quantification limits of BTTQ are more than 20 times higher, demonstrating sufficient value for practical applications.

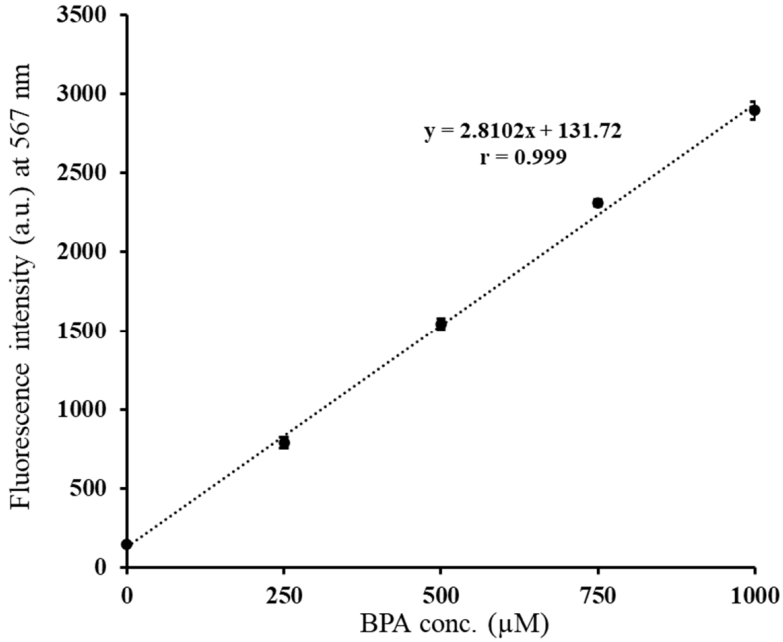


Figure 5. Correlation between fluorescence intensity and BPA concentration (0–1000 μM) of BTTQ (10 μM) in 0.5% DMSO/H_2O and linear regression analysis (FP-8600 spectrometer; λex/λem: 430/567 nm).

3.2. Selectivity Assay

Figure 6 shows the changes in the fluorescence intensity of BTTQ upon the addition of 10 equivalents of BPA or various metal chlorides. A significant fluorescence enhancement was observed only in response to BPA, while no such increase was observed for any of the tested metal cations. These results indicate that BTTQ selectively responds to BPA over metal ions. Notably, a decrease in fluorescence intensity was observed in the presence of Fe^{2+}, Fe^{3+}, and Cu^{2+}. This quenching effect is consistent with previous reports and may be attributed to static or dynamic quenching [36,37].

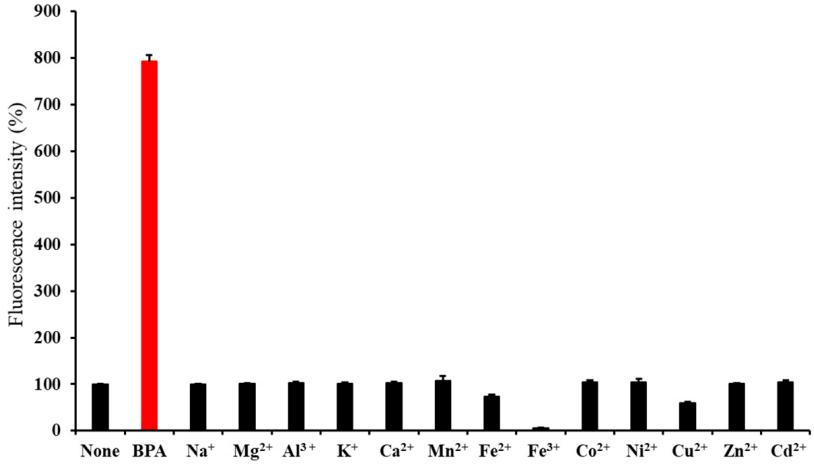


Figure 6. Fluorescence intensities (%) of BTTQ (10 μM) after the addition of BPA or various metal cations (100 μM) in 0.5% DMSO/H_2O (FP-8300 spectrometer; λex/λem: 430/567 nm).

Next, the effects of various metal cations coexisting in BTTQ and BPA were evaluated (Figure 7). Most metal cations did not inhibit the increase in fluorescence intensity, whereas

Cu^{2+}, Fe^{2+}, and Fe^{3+} suppressed the increase. Notably, the quenching effect of Fe^{3+} on the fluorescence intensity was significant. As shown in Figure S9, decreasing Fe^{3+} concentration resulted in a corresponding increase in fluorescence intensity. Given that the intracellular concentration of these metal cations is typically much lower than that of BPA, the effect is expected to be minimal [38].

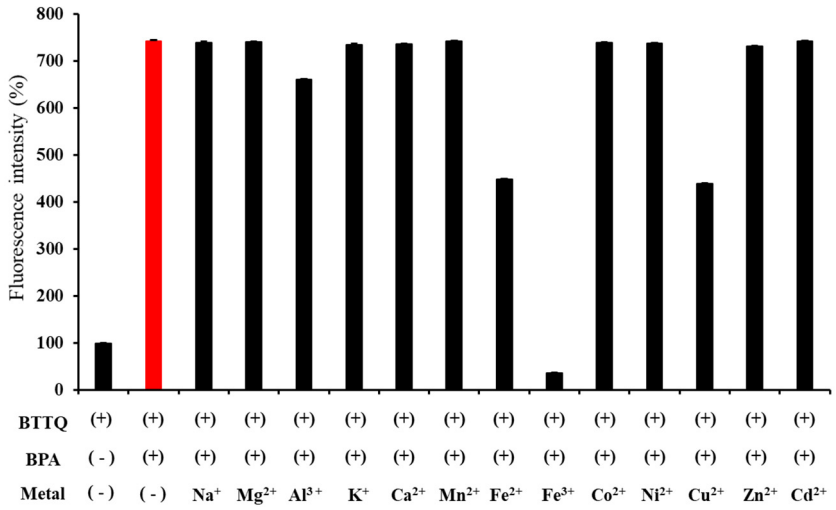


Figure 7. Fluorescence intensities (%) of BTTQ (10 μM) after the addition of BPA and competing metal cations (100 μM and 100 μM, respectively) in 0.5% DMSO/H_2O (FP-8300 spectrometer; λex/λem: 430/567 nm).

3.3. Fluorescence Microscopy Study

Fluorescence images of T3M-4 cells stained with BTTQ and Hoechst 33342, with or without BPA treatment, are shown in Figure 8. Imaging was performed using green fluorescent protein (GFP; Figure 8A,D) and DAPI (Figure 8B,E; pseudo-color: blue) filter cubes. BTTQ was efficiently excised and detected using the GFP filter cube, because its excitation spectrum overlapped well with the filter's excitation range of approximately 470 nm (Figure S4). In contrast, Hoechst 33342 requires a DAPI filter for efficient excitation. Therefore, the co-staining of intracellular boron with BTTQ and of nuclei with Hoechst 33342 was successfully achieved using both filters (Figure 8C,F). A detailed image analysis revealed that cells without BPA treatment showed only weak fluorescence in the GFP channel (Figure 8A), whereas cells treated with BPA displayed strong green fluorescence distributed throughout the cytoplasm (Figure 8D). In addition, merged images indicated that BTTQ-derived fluorescence was more intense in regions overlapping with Hoechst-stained nuclei. These results are consistent with previous findings using BS-631 and BITQ [26,27] and suggest that BTTQ can be used as a fluorescent probe to visualize the intracellular distribution of boronic-acid-containing agents. Intracellular BPA could be rapidly detected by BTTQ even at low concentrations (10 μM). This feature is advantageous in reducing the risk of cytotoxicity and other undesirable effects, especially when compared to BS-631 [27], which requires a higher concentration (100 μM) for BPA detection. In fact, preliminary studies using live human lung adenocarcinoma A549 cells revealed no apparent cytotoxicity following a 60 min treatment with 10 μM BTTQ. Moreover, BTTQ does not require cell fixation with paraformaldehyde or membrane permeabilization for imaging, allowing real-time analysis of BPA in living cells. These characteristics suggest that BTTQ is a promising tool for evaluating BNCT agents and may also be applicable to other boronic-acid-containing agents.

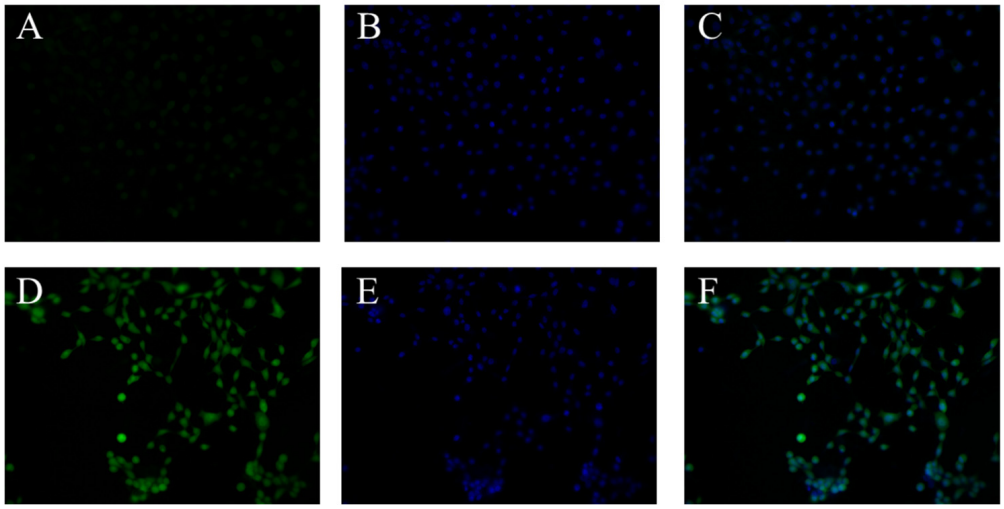


Figure 8. Fluorescence microscopic images of T3M-4 cells: group without addition of BPA (**A**–**C**), BPA additive group (**D**–**F**). (**A**,**D**) Fluorescence images after addition of BTTQ (10 μM) (GFP-filter: Ex: 470 nm ± 20 nm; Em: 525 nm ± 25 nm). (**B**,**E**) Nucleus staining using Hoechst 33342 (100 μg/mL) (DAPI-filter: Ex: 360 nm ± 20 nm; Em: 460 nm ± 25 nm). (**C**,**F**) Overlay images of fluorescence from BTTQ and Hoechst 33342.

4. Conclusions

In this study, we developed BTTQ, a boronic-acid-targeted fluorescent probe that emits light in the long-wavelength region. BTTQ retains the favorable properties of BITQ, including its low molecular weight and rapid, selective reactivity with boronic acids, while overcoming the limitations of BITQ, such as short-wavelength emission and high background fluorescence. In contrast to BS-631, BTTQ enables the detection of BPA at low concentrations without requiring cell fixation, enabling real-time monitoring of boron dynamics within living cells. These advantages make BTTQ a promising tool for evaluating boronic-acid-containing compounds, particularly in the development of next-generation BNCT therapeutics.

Supplementary Materials: The following supporting information can be downloaded at: https://www.mdpi.com/article/10.3390/chemosensors13080283/s1, Figure S1: ^{1}H NMR spectra of BTTQ (DMSO-d_6, 500 MHz); Figure S2: ^{13}C NMR spectra of BTTQ (DMSO-d_6, 125 MHz); Figure S3: EI-Mass spectra of BTTQ; Figure S4: EI-Mass spectra of BTTQ-phenylboronic acid complex; Figure S5: Excitation spectra of BTTQ (10 μM) in 0.5% DMSO/H_2O 5 min after addition of BPA (1000 μM) (FP-8600 spectrometer); Figure S6: Effect of pH on the fluorescence intensity of BTTQ (10μM) before (black line) or after (red line) addition of BPA (100μM) (FP-8300 spectrometer; λex/λem: 430/567 nm); Figure S7: (A) Emission spectra of BTTQ (10 μM) in 25% DMSO/H_2O 5 min after addition of BPA (0 or 1000 μM) (FP-8300 spectrometer; λex: 451 nm). (B) Emission spectra of BTTQ (10 μM) in 50% DMSO/H_2O 5 min after addition of BPA (0 or 1000 μM) (FP-8300 spectrometer; λex: 403 nm); Figure S8: Emission spectra of BTTQ (10 μM) in 0.5% DMSO/H_2O, measured 5 min after addition of each boronic-acid-containing compound (0 or 100 μM) (FP-8300 spectrometer; λex: 430 nm). (A) Boric acid; (B) ethylboronic acid; (C) 4-Carboxyphenylboronic acid; (D) 2-(Hydroxymethyl)phenylboronic acid cyclic monoester; Figure S9: Fluorescence intensities (%) of BTTQ (10 μM) after the addition of BPA (100 μM) and increasing concentrations of Fe^{3+} (0, 1, 10, 100 μM) in 0.5% DMSO/H_2O. (FP-8300 spectrometer; λex/λem: 430/567 nm). The fluorescence intensity of the sample containing BTTQ and BPA alone was set at 100%.

Author Contributions: Conceptualization, S.T., N.K., T.T. and M.H.; methodology, S.T., N.K., A.M. and M.H.; validation, S.T., H.D., N.K. and A.M.; formal analysis, S.T., H.D., N.K., F.H. and S.H.; investigation, S.T., H.D., A.M., F.H. and S.H.; data curation, S.T., N.K., T.T. and M.H.; writing—

original draft preparation, S.T.; writing—review and editing, S.T., N.K., T.T. and M.H.; visualization, S.T.; supervision, T.T. and M.H.; project administration, S.T., N.K., T.T. and M.H. All authors have read and agreed to the published version of the manuscript.

Funding: This study was partially supported by the Japan Society for the Promotion of Science, Japan (24K10921, 24K18844).

Institutional Review Board Statement: Not applicable.

Informed Consent Statement: Not applicable.

Data Availability Statement: The data supporting the results and findings of this study are available within the article and the Supplementary Information files. Additional raw data are available from the corresponding author upon request.

Conflicts of Interest: The authors declare no conflicts of interest.

Abbreviations

The following abbreviations are used in this manuscript:

BNCT	Boron neutron capture therapy
BPA	4-borono-L-phenylalanine
DAPI	4′,6-diamidino-2-phenylindole
HBT	2-(2-hydroxyphenyl) benzothiazole
MS	Mass spectra
HRMS	High-resolution mass spectra

References

1. Suzuki, M. Boron neutron capture therapy (BNCT): A unique role in radiotherapy with a view to entering the accelerator-based BNCT era. *Int. J. Clin. Oncol.* **2020**, *25*, 43–50. [CrossRef] [PubMed]
2. Hattori, Y.; Andoh, T.; Kawabata, S.; Hu, N.; Michiue, H.; Nakamura, H.; Nomoto, T.; Suzuki, M.; Takata, T.; Tanaka, H.; et al. Proposal of recommended experimental protocols for in vitro and in vivo evaluation methods of boron agents for neutron capture therapy. *J. Radiat. Res.* **2023**, *64*, 859–869. [CrossRef] [PubMed]
3. Barth, R.; Mi, P.; Yang, W. Boron delivery agents for neutron capture therapy of cancer. *Cancer Commun.* **2018**, *38*, 35. [CrossRef]
4. Hughes, A.; Hu, N. Optimizing Boron Neutron Capture Therapy (BNCT) to Treat Cancer: An Updated Review on the Latest Developments on Boron Compounds and Strategies. *Cancers* **2023**, *15*, 4091. [CrossRef]
5. Fukuda, H. Boron Neutron Capture Therapy (BNCT) for Cutaneous Malignant Melanoma Using 10B-p-Boronophenylalanine (BPA) with Special Reference to the Radiobiological Basis and Clinical Results. *Cells* **2021**, *10*, 2881. [CrossRef]
6. Sato, M.; Hirose, K.; Takeno, S.; Aihara, T.; Nihei, K.; Takai, Y.; Hayashi, T.; Bando, K.; Kimura, H.; Tsurumi, K.; et al. Safety of Boron Neutron Capture Therapy with Borofalan(10B) and Its Efficacy on Recurrent Head and Neck Cancer: Real-World Outcomes from Nationwide Post-Marketing Surveillance. *Cancers* **2024**, *16*, 869. [CrossRef]
7. Seneviratne, D.; Advani, P.; Trifiletti, D.; Chumsri, S.; Beltran, C.; Bush, A.; Vallow, L. Exploring the Biological and Physical Basis of Boron Neutron Capture Therapy (BNCT) as a Promising Treatment Frontier in Breast Cancer. *Cancers* **2022**, *14*, 3009. [CrossRef]
8. Detta, A.; Cruickshank, G. L-Amino Acid Transporter-1 and Boronophenylalanine-Based Boron Neutron Capture Therapy of Human Brain Tumors. *Cancer Res.* **2009**, *69*, 2126–2132. [CrossRef]
9. Sato, M.; Hirose, K. Efficacy and safety of boron neutron capture therapy for Hypopharyngeal/ Laryngeal cancer patients with previous head and neck irradiation in Japan. *Radiother. Oncol.* **2024**, *198*, 110382. [CrossRef]
10. Hirano, F.; Kondo, N.; Murata, Y.; Sudani, A.; Temma, T. Assessing the effectiveness of fluorinated and α-methylated 3-boronophenylalanine for improved tumor-specific boron delivery in boron neutron capture therapy. *Bioorg. Chem.* **2024**, *142*, 106940. [CrossRef] [PubMed]
11. Halbert, G.; Elliott, M.; Ford, S.; Dick, L.; Schmidt, E. Improved pharmaceutical stability of a boronphenylalanine mannitol formulation for boron neutron capture therapy. *Eur. J. Pharm. Sci.* **2013**, *48*, 735–739. [CrossRef]
12. Kondo, N.; Hirano, F.; Temma, T. Evaluation of 3-Borono-l-Phenylalanine as a Water-Soluble Boron Neutron Capture Therapy Agent. *Pharmaceutics* **2022**, *14*, 1106. [CrossRef]
13. Nomoto, T.; Inoue, Y.; Yao, Y.; Suzuki, M.; Kanamori, K.; Takemoto, H.; Matsui, M.; Tomoda, K.; Nishiyama, N. Poly(vinyl alcohol) boosting therapeutic potential of p-boronophenylalanine in neutron capture therapy by modulating metabolism. *Sci. Adv.* **2020**, *6*, eaaz1722. [CrossRef]

14. Konarita, K.; Kanamori, K.; Suzuki, M.; Tokura, D.; Tanaka, S.; Honda, Y.; Nishiyama, N.; Nomoto, T. Poly(vinyl alcohol) potentiating an inert D-amino acid-based drug for boron neutron capture therapy. *J. Control. Release* **2025**, *377*, 385–396. [CrossRef]
15. Toumia, Y.; Lunetta, E.; Carr, M.; Borgia, S.; Tortorella, E.; Domenici, F.; d'Agostino, E.; Telling, M.; di Fulvio, A.; Paradossi, G. Potential of BPA functionalized poly(vinylalcohol)-shelled perfluorobutane nanodroplets towards enhanced boron neutron capture therapy and in-situ dosimetry. *Appl. Mater. Today* **2024**, *36*, 102052. [CrossRef]
16. Mechetin, G.; Zharkov, D. DNA Damage Response and Repair in Boron Neutron Capture Therapy. *Genes* **2023**, *14*, 127. [CrossRef] [PubMed]
17. Seneviratne, D.; Saifi, O.; Mackeyev, Y.; Malouff, T.; Krishnan, S. Next-Generation Boron Drugs and Rational Translational Studies Driving the Revival of BNCT. *Cells* **2023**, *12*, 1398. [CrossRef]
18. Jaervinen, J.; Pulkkinen, H.; Rautio, J.; Timonen, J. Amino Acid-Based Boron Carriers in Boron Neutron Capture Therapy (BNCT). *Pharmaceutics* **2023**, *15*, 2663. [CrossRef]
19. Skwierawska, D.; López-Valverde, J.; Balcerzyk, M.; Leal, A. Clinical Viability of Boron Neutron Capture Therapy for Personalized Radiation Treatment. *Cancers* **2022**, *14*, 2865. [CrossRef]
20. Reifschneider, O.; Schütz, C.; Brochhausen, C.; Hampel, G.; Ross, T.; Sperling, M.; Karst, U. Quantitative bioimaging of p-boronophenylalanine in thin liver tissue sections as a tool for treatment planning in boron neutron capture therapy. *Anal. Bioanal. Chem.* **2015**, *407*, 2365–2371. [CrossRef]
21. Chandra, S.; Ahmad, T.; Barth, R.; Kabalka, G. Quantitative evaluation of boron neutron capture therapy (BNCT) drugs for boron delivery and retention at subcellular-scale resolution in human glioblastoma cells with imaging secondary ion mass spectrometry (SIMS). *J. Microsc.* **2014**, *254*, 146–156. [CrossRef]
22. Aldossari, S.; McMahon, G.; Lockyer, N.; Moore, K. Microdistribution and quantification of the boron neutron capture therapy drug BPA in primary cell cultures of human glioblastoma tumour by NanoSIMS. *Analyst* **2019**, *144*, 6214–6224. [CrossRef]
23. Ahmed, N.; Liu, J.; Xu, X.; Hussain, A.; Mustafai, A.; Yar, M.; Ayub, K.; Alothman, A.; Mohammad, S.; Ye, Y.; et al. An activatable NIR turn-on fluorescent probe for copper (II) ion and live cell imaging. *Sci. Rep.* **2024**, *14*, 19068. [CrossRef] [PubMed]
24. Lu, X.; Zhu, H.; Chen, Y.; Wu, Y.; Zhang, D.; Zhu, B.; Huang, S. A novel fluorescent probe for detecting hydrogen sulfide in osteoblasts during lipopolysaccharide-mediated inflammation under periodontitis. *Sci. Rep.* **2021**, *11*, 20156. [CrossRef]
25. Hagimori, M.; Karimine, Y.; Mizuyama, N.; Hara, F.; Fujino, T.; Saji, H.; Mukai, T. Selective Cadmium Fluorescence Probe Based on Bis-heterocyclic Molecule and its Imaging in Cells. *J. Fluoresc.* **2021**, *31*, 1161–1167. [CrossRef]
26. Kondo, N.; Takada, S.; Hagimori, M.; Temma, T. Development of a 2-(2-Hydroxyphenyl)-1*H*-benzimidazole-Based Fluorescence Sensor Targeting Boronic Acids for Versatile Application in Boron Neutron Capture Therapy. *Cancers* **2023**, *15*, 1862. [CrossRef] [PubMed]
27. Kondo, N.; Aoki, E.; Takada, S.; Temma, T. A Red-Emitting Fluorescence Sensor for Detecting Boronic Acid-Containing Agents in Cells. *Sensors* **2022**, *22*, 7671. [CrossRef]
28. Jie, O.; Chenguang, O.; Fujii, Y.; Nakano, Y.; Shoda, T.; Nagano, T. Synthesis and fluorescent properties of 2-(1H-benzimidazol-2-yl)-phenol derivatives. *J. Heterocycl. Chem.* **2004**, *41*, 359–365.
29. Arachchige, K.; Corbin, B.; Ediriweera, P.; Vrionides, M.; Salmon, C.; Pang, Y.; Mani, T.; Sameera, W.; Abeywickrama, C. Deprotonation-Induced Large Fluorescence Turn ON in a 2,4-Bis(benzo[d]thiazol-2-yl)phenol (HBT-BT) Derivative. *J. Phys. Chem. A* **2025**, *129*, 4189–4203. [CrossRef]
30. Kwak, M.; Kim, Y. Photostable BF2-Chelated Fluorophores Based on 2-(2′-Hydroxyphenyl)benzoxazole and 2-(2′-Hydroxyphenyl)benzothiazole. *Bull. Korean Chem. Soc.* **2009**, *30*, 2865–2866. [CrossRef]
31. Ren, T.; Xu, W.; Zhang, W.; Zhang, X.; Wang, Z.; Xiang, Z.; Yuan, L.; Zhang, X. A General Method To Increase Stokes Shift by Introducing Alternating Vibronic Structures. *J. Am. Chem. Soc.* **2018**, *140*, 7716–7722. [CrossRef] [PubMed]
32. Mao, Z.; Rha, H.; Kim, J.; You, X.; Zhang, F.; Tao, W.; Kim, J. THQ-Xanthene: An Emerging Strategy to Create Next-Generation NIR-I/II Fluorophores. *Adv. Sci.* **2023**, *10*, 2301177. [CrossRef] [PubMed]
33. Schmitt, A.; Hinkeldey, B.; Wild, M.; Jung, G. Synthesis of the Core Compound of the BODIPY Dye Class: 4,4′-Difluoro-4-bora-(3a,4a)-diaza-s-indacene. *J. Fluoresc.* **2009**, *19*, 755–758. [CrossRef]
34. Patterson, K.; Romero-Reyes, M.; Heemstra, J. Fluorescence Quenching of Xanthene Dyes during Amide Bond Formation Using DMTMM. *ACS Omega* **2022**, *7*, 33046–33053. [CrossRef] [PubMed]
35. Sun, W.; Qi, Y.; Wang, L.; Tan, Y.; Zhang, X.; Wang, J.; Li, Y. Synthesis and mechanistic investigation of BPA fluorescent probes targeting BPA for potential application in Boron Neutron Capture Therapy (BNCT). *Spectrochim. Acta Part A-Mol. Biomol. Spectrosc.* **2025**, *327*, 125318. [CrossRef]
36. Hara, F.; Mizuyama, N.; Fujino, T.; Takada, S.; Temma, T.; Saji, H.; Mukai, T.; Hagimori, M. Development of a Pyrone-Fused Tricyclic Scaffold-based Ratiometric Fluorescent Probe for Al^{3+} Detection. *J. Fluoresc.* **2024**, *35*, 4559–4568. [CrossRef]

37. Boonkitpatarakul, K.; Wang, J.; Niamnont, N.; Liu, B.; Mcdonald, L.; Pang, Y.; Sukwattanasinitt, M. Novel Turn-On Fluorescent Sensors with Mega Stokes Shifts for Dual Detection of Al^{3+} and Zn^{2+}. *ACS Sens.* **2016**, *1*, 144–150. [CrossRef]
38. Kondo, N.; Nishikubo, T.; Wakamatsu, T.; Ishikawa, H.; Nakagawa, N.; Kuramitsu, S.; Masui, R. Insights into different dependence of dNTP triphosphohydrolase on metal ion species from intracellular ion concentrations in Thermus thermophilus. *Extremophiles* **2008**, *12*, 217–223. [CrossRef]

Disclaimer/Publisher's Note: The statements, opinions and data contained in all publications are solely those of the individual author(s) and contributor(s) and not of MDPI and/or the editor(s). MDPI and/or the editor(s) disclaim responsibility for any injury to people or property resulting from any ideas, methods, instructions or products referred to in the content.